Consistency between functional and structural networks of coupled nonlinear oscillators

Weijie Lin, Yafeng Wang, Heping Ying, Ying-Cheng Lai, and Xingang Wang

Consistency between functional and structural networks of coupled nonlinear oscillators

Weijie Lin,[1,2] Yafeng Wang,[2,3] Heping Ying,[1] Ying-Cheng Lai,[4] and Xingang Wang[2,3,*]

[1]*Department of Physics, Zhejiang University, Hangzhou 310027, China*
[2]*School of Physics and Information Technology, Shaanxi Normal University, Xi'an 710062, China*
[3]*Institute of Theoretical & Computational Physics, Shaanxi Normal University, Xi'an 710062, China*
[4]*School of Electrical, Computer, and Energy Engineering, Arizona State University, Tempe, AZ 85287, USA*

In data based reconstruction of complex networks, dynamical information can be measured and exploited to generate a functional network, but is it a true representation of the actual (structural) network? That is, when do the functional and structural networks match and is a perfect matching possible? To address these questions, we use coupled nonlinear oscillator networks and investigate the transition in the synchronization dynamics to identify the conditions under which the functional and structural networks are best matched. We find that, as the coupling strength is increased in the weak-coupling regime, the consistency between the two networks first increases and then decreases, reaching maximum in an optimal coupling regime. Moreover, by changing the network structure, we find that both the optimal regime and the maximum consistency will be affected. In particular, the consistency for heterogeneous networks is generally weaker than that for homogeneous networks. Based on the stability of the functional network, we propose further an efficient method to identify the optimal coupling regime in realistic situations where the detailed information about the network structure, such as the network size and the number of edges, is not available. Two real-world examples are given: cortico-cortical network of cat brain and the Nepal power grid. Our results provide new insights not only into the fundamental interplay between network structure and dynamics, but also into the development of methodologies to reconstruct complex networks from data.

I. INTRODUCTION

The interplay between functions and structure in complex dynamical systems is one of the central problems in interdisciplinary research [1]. Structural connectivity is referred to as the physical connections among the units in a complex system, which provides the basis for generating various collective behaviors, e.g., the anatomical connections of mammalian brains as detected by techniques such as high-resolution magnetic resonance (MR) and diffusion tensor imaging (DTI). Functional connectivity, on the other hand, is characterized by the statistical and dynamical dependencies among the unit activities, such as the correlations, synchronization/coherence, transfer entropy, etc., which can be extracted from data collected through functional magnetic resonance imaging (fMRI), electroencephalography (EEG), and multi-electrode array (MEA), etc. Functional connectivity is descriptive and is mainly used to classify and distinguish the observed phenomena [2]. The relationship between structural and functional connectivities can be highly nontrivial and quite sophisticated. In particular, as a manifestation of the collective dynamical behaviors, functional connectivity is dependent upon the detailed interaction patterns among the units, a point that has been well addressed in recent studies of network dynamics [3–5]. However, functional connectivity is not determined entirely by the structural connectivity. There are in fact circumstances in which the functional connections can be established between units without direct physical connections [6], leading to phenomena such as partial synchronization [7], noise-induced coherence [8], generalized and driven synchronization [9], etc. The nontrivial interplay between structural and functional connectivities raises a challenging question: how to infer the physical connections from the measured data of dynamical activities, referred to as the inverse problem in complex systems [10–17].

Networks of coupled nonlinear oscillators serve as a paradigmatic model to address the inverse problem. The past decade has witnessed a great deal of progress in this area of research [11–23]. In a general setting, an ensemble of nonlinear oscillators (nodes) are coupled through a complicated pattern, giving rise to various collective behaviors at the system level. The goal is to retrieve from the measured dynamical data or time series the detailed structural information about the underlying network, such as the modular structure [19, 22], network symmetries [24], and nodal degrees [25], etc. In a real-world system, the functional connectivity can be assessed through calculating the correlation coefficients among the nodal dynamics [2]. Naturally, the synchronous dynamics of the network plays a crucial role in revealing the relationship between functional and structural connectivities [6]. In the past, a variety of synchronization-based methods were proposed for reconstructing the structural connectivity from observed nodal dynamics [18–24]. For instance, through an adaptive feedback approach [18], the structure of a complex network can be "copied" to an auxiliary network if the two networks can be synchronized. In Ref. [19], transient synchronization is exploited to reveal the modular structures of complex networks, which emerges spontaneously in distinct time scales of the dynamical evolution. In Ref. [21], it was found that, by driving a synchronized network with constant external input signals, the network connectivity can be deduced from the stationary pattern of network desynchronization. In Ref. [22], the cat

*Email address:wangxg@snnu.edu.cn

cortex was modeled as a network of subnetworks consisting of noisy excitable neurons and it was found that in the biologically plausible regime (typically the regime of weak coupling strength), the anatomical community structures on different scales can be successfully retrieved from the functional clusters defined according to the synchronization dynamics.

The interplay between synchronization and network reconstruction, however, can be quite subtle [6]. Take the network of diffusively coupled nonlinear oscillators as an example [4, 5]. If the coupling strength is too weak, no oscillators in the network are synchronized, regardless of whether there are direct connections. As a result, no information about the network structure can be obtained from the nodal activities. If the coupling strength is too strong, most oscillators will be synchronized, generating identical dynamical trajectories. In this case, no information about the network structure can be obtained either. The "double-sword" role of synchronization in network construction justifies the following question: *when do synchronization behaviors best reflect the structural connectivity of the network?* From the standpoint of synchronization transition, this question can be interpreted as finding the optimal coupling, or the optimal coupling regime, in which the functional and structural connectivities are best matched. Previous studies of synchronization-based network reconstruction provided some hints, but these were mainly based on some specific features of the system dynamics, leading sometimes to inconsistent conclusions. For instance, in contrast to the finding that structural connectivity is better assessed in a more pronounced synchronization regime (e.g., the methods based on transient synchronization and driving-induced dynamical responses [19, 21]), in Refs. [22, 23], it was shown that for neuronal systems such as cat brain, the structural connectivity can be retrieved but only in the asynchronous regime.

In this paper, we investigate the consistency between the functional and structural networks using coupled nonlinear oscillator networks in the weakly coupling regime, with a focus on searching for the optimal coupling regime where the two networks are best matched. We find that, when the nodal dynamics are asynchronous, such an optimal coupling regime generally exists, in spite of the dependence of the details of this regime on nodal dynamics and network structure. An interesting phenomenon is that the consistency of heterogeneous networks is generally weaker than that for homogeneous networks. Taking advantage of the stability of the functional network, we articulate and validate an efficient procedure to identify the optimal coupling regime from time series. Our work not only gives new insights into the interplay between network structure and dynamics, but also provides a practical method to identify the optimal coupling regime that maximizes the structural and functional consistency. This may have potential applications in fields such as biomedicine.

In Sec. II, we describe the model of coupled-oscillator networks, define the functional network, demonstrate variations in the network consistency, and show the existence of the optimal coupling regime. In Sec. III, we study the impact of network structure on consistency. In Sec. IV, we present a data-based method to identify the optimal coupling, assuming that the network structure is unknown. In Sec. V, we extend our study to alternative network models, taking into account variations in network size and nodal dynamics, and to two real-world networks as well: the cortico-cortical network of cat brain and the Nepal power grid. In Sec. VI, we present conclusions and discussions.

II. MODEL DESCRIPTION AND NUMERICAL RESULTS

We consider the following network model of coupled nonlinear oscillators:

$$\dot{\mathbf{x}}_i = \mathbf{F}(\mathbf{x}_i) - \varepsilon \sum_{j=1}^{N} a_{ij}[\mathbf{H}(\mathbf{x}_j) - \mathbf{H}(\mathbf{x}_i)], \qquad (1)$$

where $i, j = 1, \ldots, N$ are the oscillator (node) indices, $\mathbf{x}$ is an n-dimensional state vector, and ε denotes the coupling strength. The individual nodal dynamics is assumed to be identical and described by $\dot{\mathbf{x}} = \mathbf{F}(\mathbf{x})$, and $\mathbf{H}(\mathbf{x})$ is the coupling function. The coupling relationship among the oscillators, i.e., the structural connectivity, is characterized by the adjacency matrix $\mathbf{A}$, where $a_{ij} = 1$ if nodes i and j are directly connected, and $a_{ij} = 0$ otherwise. This model of linearly coupled nonlinear oscillators and its variants are standard in the literature of network synchronization [4, 5], which has been widely used to gain insights into the interplay between network structure and dynamics, as well as to test synchronization-based methods for network reconstruction [13–15, 18, 23–25].

For neuronal systems such as the human brain, the mean activity of the population of neurons in a small area normally has a broad frequency spectrum but with some pronounced rhythms [26]. Motivated by this, we assume the nodal dynamics to be chaotic. Specifically, we define the nodal activities as those determined by the chaotic logistic map, $x(n + 1) = F[x(n)] = 4x(n)[1 - x(n)]$, and set the coupling function as $H(x) = F(x)$. (As will be discussed later, our main results do not depend on the specific nodal dynamics.) We note that, in previous studies of coupled periodic oscillator systems, the network structure cannot be retrieved in the weakly coupling regime [22, 23].

To be concrete, we investigate the consistency of functional and structural connectivities in small-world networks (SWNs). We choose the coupling strength randomly in the asynchronous regime. SWNs of $N = 50$ nodes and average degree $\langle k \rangle = 6$ (so the total number of links is $L = N\langle k \rangle/2 = 150$) are generated using the standard rewiring algorithm [3] with the rewiring probability $\rho = 0.1$. In simulations, we choose the initial conditions of the logistic maps randomly from the unit interval and, after a transient period of 5×10^3 iterations, construct the functional network based on Pearson's correlation. More specifically, we record the states of all maps in the network for a period of $T = 2 \times 10^3$ iterations, and calculate the correlation coefficient between maps i and j using

the formula,

$$r_{ij} = \frac{\sum_{n=1}^{T}(x_i(n)-\bar{x}_i)(x_j(n)-\bar{x}_j)}{\sqrt{\sum_{n=1}^{T}(x_i(n)-\bar{x}_i)^2 \sum_{n=1}^{T}(x_j(n)-\bar{x}_j)^2}}, \quad (2)$$

where $\bar{x} = \sum_{n=1}^{T} x(n)/T$ is the time-averaged dynamical variable. We then average r_{ij} over an ensemble of initial conditions and calculate the corresponding ensemble-averaged correlation coefficient c_{ij}. Because the correlation matrix $\mathbf{C}$ is symmetric, we only need to keep elements in the upper triangular part, i.e., we can set $c_{ij} = 0$ for $i \geq j$ in $\mathbf{C}$. Finally, we select from $\mathbf{C}$ the L largest elements (so as to make the size and the total number of links in the functional network identical to those of the structural network), which give the respective functional links. These links, together with the nodes they connect with, constitute the functional network.

To evaluate the consistency between the functional and structural networks, we introduce a quantitative measure: the similarity coefficient $S = \sum_{l=1}^{L} s_l/L$, with s_l being the consistency of the lth link. Specifically, we have $s_l = 1$ if the lth link of the structural network is also a link of the functional network, otherwise we have $s_l = 0$. Note that, through defining the similarity coefficient, we treat the functional links effectively as unweighted and undirected, i.e., the functional network can also be described by a binary matrix. In general, we have $0 \leq S \leq 1$, and a larger value of S indicates a higher degree of consistency between the two networks. For $S = 1$, the two networks are completely matched, making it possible to infer the structural connectivity precisely from the functional connectivity.

We evaluate the consistency between the functional and structural networks in the weakly coupling regime in which synchronization is unlikely. We choose ε randomly in the range $\varepsilon \in (0, \varepsilon_c)$, with ε_c being the critical coupling strength marking the onset of network synchronization. (Note that ε_c can be estimated through an eigenvalue analysis [27, 28].) For our SWN model, we have $\varepsilon_c \approx 5 \times 10^{-2}$. The network consistency for four typical coupling strengths are presented in Fig. 1. For $\varepsilon = 1 \times 10^{-3}$ [Fig. 1(a)], the functional network appears quite different from the structural network. Indeed, the similarity coefficient for this case is $S = 0.37$. Raising the coupling strength to 2×10^{-3} [Fig. 1(b)], we see that the overlap between the two networks is increased, leading to $S = 0.77$. For $\varepsilon = 1 \times 10^{-2}$ [Fig. 1(c)], remarkably the functional network overlaps with the structural network completely, giving rise to $S = 1$. Increasing ε further to 2×10^{-2} [Fig. 1(d)], the degree of consistency between the two networks is reduced, corresponding to $S = 0.61$.

To better understand the physical meaning of the network consistency, we plot in Fig. 1(e) the probability distributions of c_{ij} for the values of the coupling strength used in Figs. 1(a-d), which provide additional information about the functional connections. In fact, this distribution is key to network reconstruction [14, 17, 22]. To accurately reconstruct the structural network from the functional network, it is required that the correlation coefficient should have a bimodal distribution, with one peak corresponding to existent links and another to nonexistent ones. Thus, if the two peaks are well separated,
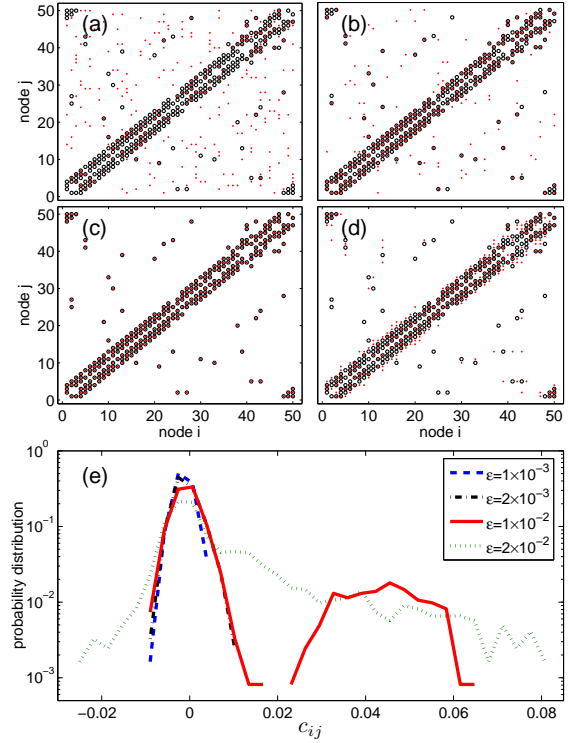

FIG. 1: (Color online) For SWNs of coupled chaotic logistic maps, (a-d) consistency between the functional (red dots) and structural (open circles) networks and (e) the probability distributions of the correlation coefficient c_{ij} for different coupling strengths. The parameters are (a) $\varepsilon = 1 \times 10^{-3}$, $S = 0.37$, (b) $\varepsilon = 2 \times 10^{-3}$, $S = 0.77$, (c) $\varepsilon = 1 \times 10^{-2}$, $S = 1$, and (d) $\varepsilon = 2 \times 10^{-2}$, $S = 0.61$. The results are averaged over 20 system realizations.

the reconstruction accuracy will be higher. However, if the distribution is unimodal, it will be difficult to distinguish the actual links from the nonexistent ones, making it difficult to infer the network structure. From Fig. 1(e), we see that, for $\varepsilon = 1 \times 10^{-2}$, the distribution consists of two well separated peaks. However, for other coupling strengths the distributions are either unimodal ($\varepsilon = 1 \times 10^{-3}$ and 2×10^{-3}) or bimodal but with indistinguishable peaks ($\varepsilon = 2 \times 10^{-2}$). These results are consistent with Figs. 1(a-d).

Figure 1 indicates that, for properly chosen coupling strength, the structural connectivity can be reliably retrieved for coupled chaotic oscillator networks. This result extends those in Refs. [22, 23], where it was shown that in the weakly coupling regime the structural connectivity can only be retrieved in excitable networks of coupled noisy neurons. Figure 1 also shows that, in the asynchronous regime, there exists an optimal coupling value (about $\varepsilon_o = 1 \times 10^{-2}$) for which the functional network matches perfectly with the structural network: $S = 1$. The general existence of the optimal coupling value and its dependence on the network structure are issues to be addressed next.
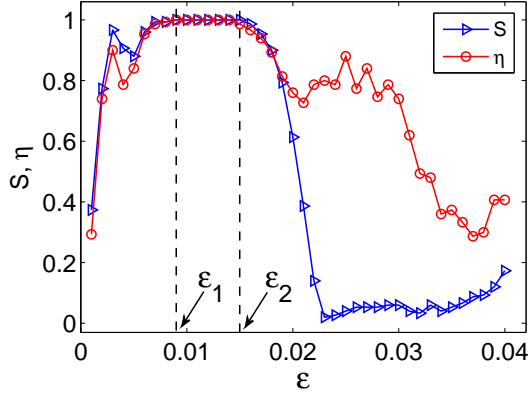
FIG. 2: (Color online) For SW networks, the network similarity coefficient (open triangles) S and the link stability coefficient (open circles) η versus the coupling strength ε. Both S and η reach unity values for $\varepsilon \in [\varepsilon_1, \varepsilon_2]$, where $\varepsilon_1 \approx 9 \times 10^{-3}$ and $\varepsilon_2 \approx 1.5 \times 10^{-2}$. The results are averaged over 20 system realizations.

III. EFFECTS OF NETWORK STRUCTURE ON CONSISTENCY

To better reveal the optimal coupling regime, we vary the coupling strength ε in the range $(0, 4 \times 10^{-2})$ and calculate the similarity coefficient S as a function of ε. The results are presented in Fig. 2. We see that, as ε is increased from zero, S first increases, reaches its maximally possible value ($S = 1$) for $\varepsilon_1 = 9 \times 10^{-3}$, remains at the unity value until ε passes through $\varepsilon_2 \approx 1.5 \times 10^{-2}$. As ε is increased further from ε_2, S quickly decreases to near zero values. Figure 2 shows, strikingly, that there actually exists an interval in the parameter space, $\varepsilon \in [\varepsilon_1, \varepsilon_2]$, in which the functional and structural networks are perfectly matched.

The existence of an optimal coupling regime in which the functional and structural networks match perfectly is remarkable, but does this hold for network topologies other than the small world, e.g., random networks (RNs) and scale-free networks (SFNs) [29]? Setting the rewiring probability to be $\rho = 1$ in the SWN model, we effectively generate RNs [3] and can then investigate the variations of the network consistency in the weak-coupling regime ($\varepsilon_c \approx 4.2 \times 10^{-2}$). The results are presented in Fig. 3(a). We find that, as for the case of SWNs, there exists an coupling interval, $\varepsilon \in [\varepsilon_1 \approx 8 \times 10^{-3}, \varepsilon_2 \approx 1.2 \times 10^{-2}]$, within which the functional and the structural networks match perfectly. Comparing with the results for SWNs, we observe similar behaviors in the variations of S with ε.

Keeping the network size and the total number of connections unchanged, we study SFNs generated according to the standard BA algorithm [30]. The network consistency measure S versus the coupling strength in the weak-coupling regime is shown in Fig. 3(b) ($\varepsilon_c \approx 2.5 \times 10^{-2}$ for SFN). Comparing with the results of SWNs and RNs, we notice a distinct feature for SFNs in that the structural connectivity cannot be perfectly retrieved: $S_{max} \approx 0.985 < 1$ for $\varepsilon_o = 7 \times 10^{-3}$. The main reason is that SFNs have a heterogeneous degree
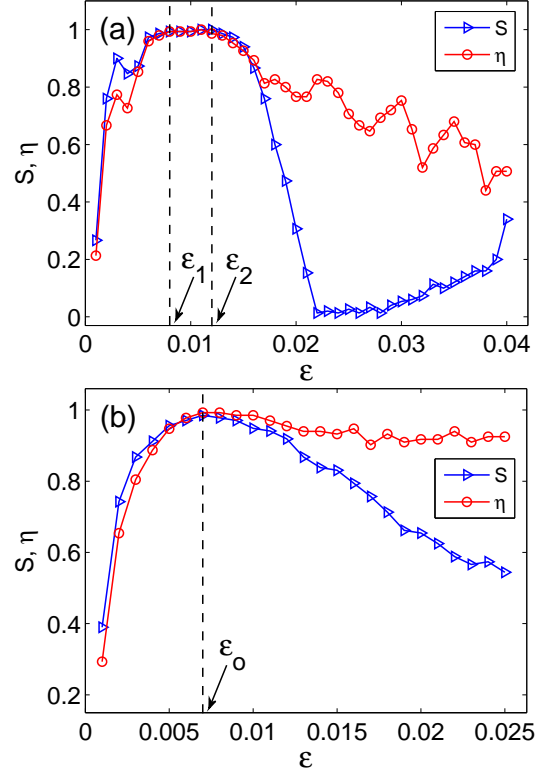

FIG. 3: (Color online) Network similarity coefficient (open triangles) S and the link stability coefficient (open circles) versus the coupling strength ε for (a) RNs and (b) SFNs. In (a), $S = \eta = 1$ is reached for $\varepsilon \in [\varepsilon_1, \varepsilon_2]$, with $\varepsilon_1 \approx 8 \times 10^{-3}$ and $\varepsilon_2 \approx 1.2 \times 10^{-2}$. In (b), we have $S_{max} \approx 0.985$ and $\eta_{max} \approx 0.993$ for $\varepsilon_o = 7 \times 10^{-3}$. Each data point is averaged over 20 system realizations.

distribution with a small number of hub nodes of extraordinarily large degrees. The network structure can thus affect the maximum consistency value. In particular, for heterogeneous networks, it is not possible to obtain perfect reconstruction of the network structure based on functional (dynamical) data.

To gain more insights into the deterioration of the network consistency in SFNs, we examine the mismatched connections in the functional network for the optimal coupling strength ε_o and check the properties of the nodes they connect in the structural networks. We find that, for $\varepsilon = \varepsilon_o$, there is only one mismatched edge between the two networks and, interestingly, this edge connects the two largest hub nodes in the structural network: the 2nd node of degree $k_2 = 16$ and the 5th node of degree $k_5 = 19$. Checking their neighboring nodes in the structural network, we further find that the two hub-nodes have only 5 common neighbors, i.e., the two hubs are embedded in quite different local "environment". Since the coupling strength is weak and oscillators in the network are not synchronized, the accumulating coupling signal that each hub receives depends on the states of its neighbors. A smaller overlap in their neighborhoods leads to a larger difference in the coupling signals that they receive, leading to weaker correlation between the two hubs. This provides a heuristic explanation for the observed small correlation coef-
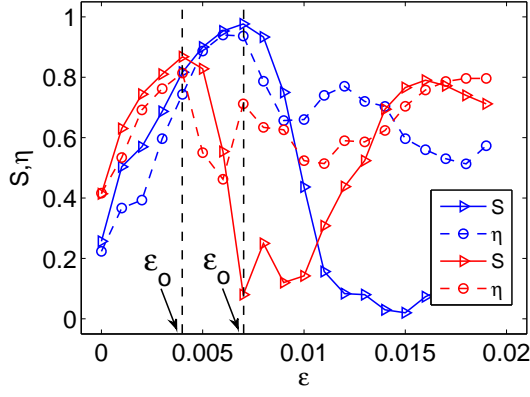
FIG. 4: (Color online) For RNs of $N = 50$ and different connection density, variations in the network similarity coefficient (open triangles) S and the link stability coefficient (open circles) as a function of the coupling strength ε. For $\langle k \rangle = 12$ (blue color), we have $S_{max} \approx 0.977$ and $\eta_{max} \approx 0.937$ for $\varepsilon_o = 7 \times 10^{-3}$. For $\langle k \rangle = 20$ (red color), we have $S_{max} \approx 0.868$ and $\eta_{max} \approx 0.814$ for $\varepsilon_o = 4 \times 10^{-3}$. Each data point is averaged over 20 system realizations.

ficient between the two hub-nodes ($c_{2,5} \approx 1 \times 10^{-3}$).

There can be also opposite situations where the hubs are not structurally connected but are functionally connected. This occurs when the neighboring nodes of two hubs are heavily overlapped. (An example of this behavior will be presented in Sec. V, where the network consistency of a cat brain network is analyzed). According to the mechanism of generalized synchronization, two uncoupled chaotic oscillators can still be synchronized if they are driven by a strong, common signal [9, 31]. As a result, although the two hubs are not structurally connected, their activities can still be highly correlated if their neighbors have a substantial overlap. The results in Fig. 3(b)] thus suggest that, comparing with the connections among the low-degree nodes, the links among the hub nodes are more difficult to be detected and ascertained. In general, network consistency is relatively weak for heterogeneous and dense networks as compared with homogeneous and sparse networks.

Our above reasoning based on neighborhood overlap is justified by numerical simulations. In particular, keeping the network size unchanged ($N = 50$), we plot in Fig. 4 the variation of S as a function of ε for RNs of $\langle k \rangle = 12$ and 20. Comparing with the result of $\langle k \rangle = 6$ [Fig. 3(a)], we see that, as $\langle k \rangle$ is increased, the network consistency is gradually deteriorated. For $\langle k \rangle = 6$, we have $S = 1$ within the interval $\varepsilon \in [8 \times 10^{-3}, 1.2 \times 10^{-2}]$, but for $\langle k \rangle = 12$ and 20, we have $S_{max} \approx 0.977$ and 0.868, respectively. Since the neighborhood overlap is enhanced in more densely connected networks, these results thus suggest that the network consistency tends to be weaker in heterogeneous and dense networks. From Figs. 3 and 4, we also observe that, with the increase in $\langle k \rangle$, the optimal coupling regime shifts towards small values, which can be attributed to the increased network synchronizability in densely connected networks.

IV. DATA-BASED IDENTIFICATION OF OPTIMAL COUPLING REGIME

While at the optimal coupling strength the functional and structural networks are best matched, it remains a challenge to identify this optimal coupling strength in a practical situation, since *a priori* knowledge of the network structure is generally not available, e.g., the structures of biological and neuronal complex networks. (We still assume that the network size and the total number of connections are known.) For the task of network reconstruction, it is desired that the optimal coupling can be evaluated from only the measured time series, so that the network structure can be best retrieved from the functional network. Based on recent works on synchronization dynamics in complex networks, we articulate an efficient method that enables reliable identification of the optimal coupling regime without knowing the network structure.

Recent studies of network synchronization demonstrated that, in an asynchronous regime where a synchronization solution between any pair of oscillators is unstable, some synchronization clusters can still emerge [32]. For example, in the weakly coupling regime where complete synchronization is ruled out, the oscillators can be phase-synchronized into different clusters, forming distinct synchronization patterns [33]. The patterns can be unstable, emerge and disappear in an intermittent fashion, but the structure of each individual cluster can still be relatively stable, depending on the network structure [7, 34]. The relation between synchronization pattern and network structure provides an approach to identifying the optimal coupling regime based on the stabilities of the synchronization patterns. In particular, through continuous variations in the coupling strength in the asynchronous regime, we can assess the stability of the constructed functional network. The optimal coupling regime is one in which the stabilities change little. This is essentially a method of *connectivity stability analysis* (CSA).

The working of our CSA method can be described as follows. First, starting from a small coupling strength close to zero, e.g., $\varepsilon = 1 \times 10^{-4}$, we construct the functional network according to the method introduced in Sec. II. Second, we apply a small increment to the coupling strength, $\Delta\varepsilon$, simulate the system evolution, and construct the functional network again. Comparing the structures of the two functional networks at slightly different values of the coupling strength, we can calculate the connectivity stability coefficient defined as $\eta = L_m/L$, where L_m is the number of matched connections between the two functional networks. Third, we increase ε progressively in the weak-coupling regime and obtain the dependence of η on ε. The optimal coupling regime is the small interval about the point at which η is maximized. *We emphasize that, unlike the quantity S, η can be calculated without the knowledge of the network structure (only the network size and the total number of connections are known). If η is maximized for the same value of ε_o that maximizes S, the full structure of the network can be obtained from the functional network.*

We now use the network models studied in Sec. III to demonstrate that the measure η can be maximized with respect to variation in the coupling strength. As shown in Fig. 2, we

see that, for SWNs, η can reach its maximum value of unity in the interval $\varepsilon \in [\varepsilon_1, \varepsilon_2]$, in remarkable agreement with the behavior of the similarity measure S, indicating that the connectivity stability coefficient is indeed able to characterize the network consistency. Similar results are also obtained for RNs and SFNs, as shown in Fig. 3. In all cases we find that η reaches its maximum at the same point at which S is maximized.

Comparing with the conventional methods of network reconstruction [11–23], our CSA method can extract the structural information of an oscillatory network in the weakly coupling regime in which many biological networks operate. Take the neuronal network as an example. To retrieve the network structure, the coupling strength among the neurons can be adjusted systematically within the biologically plausible regime through, e.g., drug delivery or external stimulations [35]. From the measured data of neuronal activities, we can construct the functional network for a set of values of the coupling strength. The stabilities of the corresponding functional network can then be calculated to yield the optimal coupling regime. The functional network in the optimal coupling regime can be taken as a good approximation of the actual structural network.

V. APPLICATION TO REAL-WORLD NETWORKS

How about realistic networks? To investigate, we check the consistency of functional and structural connectivity for two typical networks in natural and and man-made systems, namely the cortico-cortical network of cat brain and the Nepal power grid.

We first study the cat brain network, which consists of 53 nodes (cortex areas) and 519 links (fiber connections of different axon densities). The network possesses an apparent small-world feature [36]. According to their functions, the cortex areas can be grouped into four divisions: 16 areas in the visual division, 7 areas in the auditory division, 16 areas in the somatomotor division, and 14 areas in the frontolimbic division. As areas within the same division are more densely connected than from different divisions, the network possesses also the community feature [36].

Using the structure of the cortico-cortical network of cat brain, we simulate the system evolution according to Eq. (1) and examine the consistency between the functional and structural networks. The results are shown in Fig. 5(a), where the coupling strength ε is systematically changed from 0 to 1×10^{-2} (for the cat brain network, the onset of network synchronization occurs for $\varepsilon_c \approx 1.3 \times 10^{-2}$). We see that, similar to the theoretical network models, there exists an optimal coupling strength: $\varepsilon_o \approx 3.5 \times 10^{-3}$ at which the network consistency is maximized ($S_{max} \approx 0.89$). Figure 5(a) also shows the connectivity stability coefficient versus the coupling strength, which is maximized for the same value of the coupling strength ($\eta_{max} \approx 0.86$).

When checking the mismatched connections, we find that they are mostly associated with the hub nodes in the structural network. In our SFN model, we obtain that the two largest
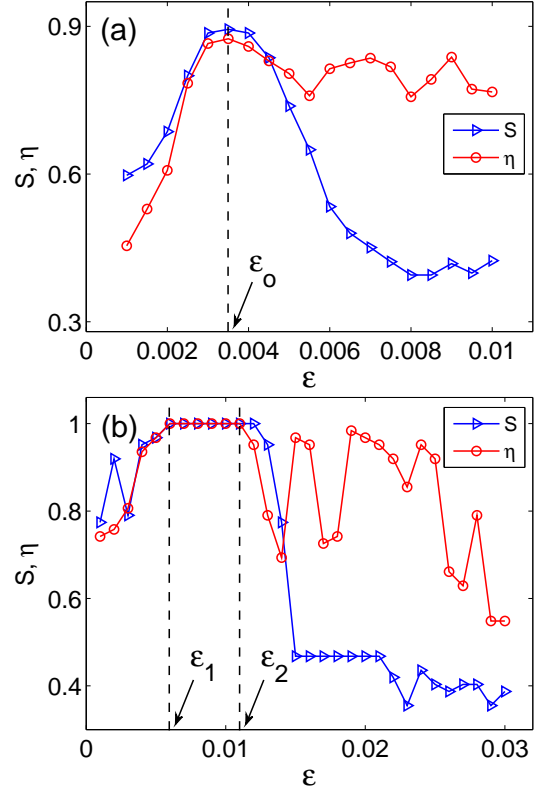

FIG. 5: (Color online) Network consistency in real-world networked systems. (a) For the cortico-cortical network of cat brain, S (open triangles) and η (open circles) versus the coupling strength. The optimal coupling strength is $\varepsilon_o \approx 3.5 \times 10^{-3}$. (b) For the Nepal power grid, the maximum values of S and η are achieved within the interval $\varepsilon \in [\varepsilon_1, \varepsilon_2]$, where $\varepsilon_1 \approx 6 \times 10^{-3}$ and $\varepsilon_2 \approx 1.1 \times 10^{-2}$. Each data point is averaged over 20 system realizations.

hubs are structurally connected but functionally disconnected. Here we observe the opposite case: two hubs that are structurally disconnected but functionally connected. These are the 43th node (in the frontolimbic division, with $k_{43} = 32$ connections) and the 44th node with $k_{44} = 34$ connections. While the two hub nodes are not directly connected, they have in total 31 common neighbors, i.e., their neighborhoods are heavily overlapped. Our reasoning in Sec. III suggests overlapping neighborhoods as the source of correlation between the dynamical activities of the two hub nodes (the correlation coefficient is $c_{43,44} \approx 2 \times 10^{-2}$), resulting in the false link in the functional network that does not exist in the structural network.

The Nepal power grid has 15 nodes (power stations) and 62 links (transmission lines) [37]. Onset of synchronization occurs for $\varepsilon_c \approx 3.6 \times 10^{-2}$. Figure 5(b) shows S and η versus the coupling strength. The optimal coupling interval is identified to be $\varepsilon \in [6 \times 10^{-3}, 1.1 \times 10^{-2}]$, in which both S and η reach their maximum values: $S = 1$ and $\eta = 1$.

We now examine the robustness of the existence of maximum consistency between the functional and structural networks with respect to changes in the system details such as the
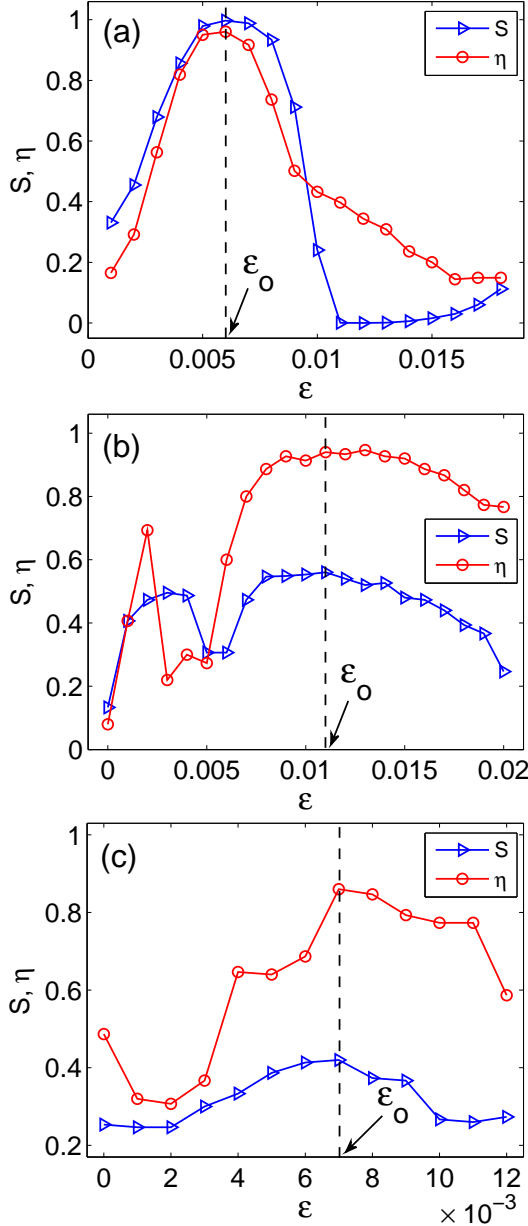
FIG. 6: (Color online) For different network models, S (open triangles) and η (open circles) versus the coupling strength: (a) RN of $N = 500$ and $\langle k \rangle = 6$ where we have $\varepsilon_o \approx 6 \times 10^{-3}$, $S_{max} \approx 0.997$, and $\eta_{max} \approx 0.961$, (b) RN of coupled chaotic Rössler oscillators, where we have $\varepsilon_o \approx 1.1 \times 10^{-2}$, $S_{max} \approx 0.56$, and $\eta_{max} \approx 0.94$, (c) RN of coupled noisy phase oscillators, where we have $\varepsilon_o \approx 7 \times 10^{-3}$, $S_{max} \approx 0.42$, and $\eta_{max} \approx 0.86$. Each data point is the result of averaging over 20 system realizations.

network size and nodal dynamics. First, we increase the size of the RN to $N = 500$ (fixing $\langle k \rangle = 6$). Onset of synchronization occurs for $\varepsilon_c = 2.2 \times 10^{-2}$. Figure 6(a) shows S and η versus ε. We see that, similar to behaviors in the smaller-size networks, there exists an optimal coupling, $\varepsilon_o = 6 \times 10^{-3}$, at which both S and η are maximized: $S_{max} \approx 0.997$ and $\eta_{max} \approx 0.961$. To investigate the effect of the nodal dynam-

ics type, we replace the logistic map with the chaotic Rössler oscillators [38] $[(dx/dt, dy/dt, dz/dt)^T = (-y - z, x + 0.1y, 0.1 + xz - 18z)^T]$ in the same RN as in Fig. 3(a), and show in Fig. 6(b) S and η versus ε. The oscillators are coupled through the x component, i.e., $\mathbf{H}([x, y, z]^T) = [x, 0, 0]^T$, and the correlation coefficient is calculated from the x component. The synchronization onset occurs for $\varepsilon_c \approx 2.0 \times 10^{-2}$. Figure 6(b) shows the existence of the optimal coupling value in the weak-coupling regime: $\varepsilon_o \approx 1.1 \times 10^{-2}$, at which both the network consistency and connectivity stability are maximized ($S_{max} \approx 0.56$ and $\eta_{max} \approx 0.94$).

The phenomenon of network consistency has also been observed in complex networks of coupled phase oscillators. In particular, we consider the generalized Kuramoto model described by [39]

$$\dot{\theta}_i = \omega_i + \varepsilon \sum_j a_{ij} \sin(\theta_j - \theta_i) + D\xi_i(t),$$

where ω_i is the natural frequency of the ith oscillator, which is randomly chosen in the range $[-0.1, 0.1]$, $\xi_i(t) \in [0, 1]$ represents independent Gaussian white noise, and D is the noise amplitude. In simulations, we fix $D = 1 \times 10^{-2}$ and choose the initial phases of the oscillators randomly from the interval $[-\pi, \pi]$. Using the same random-network structure as in Fig. 3(a), we calculate the variations in S and η as a function of ε. Figure 6(c) shows that, there exists an optimal coupling strength ($\varepsilon_o \approx 7 \times 10^{-3}$) for which both network consistency and connectivity stability are maximized ($S_{max} \approx 0.42$ and $\eta_{max} \approx 0.86$). This result is consistent with those in Ref. [39], where it was shown that, using the approach of phase synchronization, the network consistency (network similarity measure) can be maximized for some weak coupling strength.

VI.   DISCUSSIONS AND CONCLUSION

A few remarks are in order. First, our numerical results show that, despite variations in the network structure and nodal dynamics, there always exists an optimal coupling regime (interval) in which the consistency between the network functions and structure is maximized. It is useful to develop a more quantitative understanding of the mechanism that leads to this phenomenon. In Ref. [14], a relationship was established between the dynamical correlations and the topology for general coupled oscillator networks. Specifically, it was found that, in the presence of noise, there exists a one-to-one correspondence between the correlation matrix $\mathbf{C}$ (which can calculated solely from measured time series) and the network adjacency matrix $\mathbf{A}$, as

$$\mathbf{A} = \left[\sigma^2/(2\varepsilon)\right] \mathbf{C}^{\dagger},$$

where σ denotes the noise amplitude and $\mathbf{C}^{\dagger}$ is the pseudo inverse of $\mathbf{C}$. This relation provides a mechanism for the existence of the optimal coupling. In particular, if the coupling is too weak ($\varepsilon \approx 0$), the oscillators will not be correlated so that many elements of $\mathbf{C}$ will be near zero. In this case, there is a

high probability that the inverse $\mathbf{C}^{-1}$ is not well defined, defying any meaningful correspondence between the correlation matrix and the network adjacency matrix. In the other extreme case, if the coupling is too strong ($\varepsilon \ll 1$), all oscillators in the network will be synchronized so that many elements in $\mathbf{C}$ will be closing to unity. In this case, $\mathbf{C}^{-1}$ cannot be defined either. Thus, a meaningful relation between the network correlation and adjacency exists only when the coupling is neither too weak nor too strong, implying the existence of an optimal regime that maximizes the consistency between structural and functional networks.

Second, from numerical simulations, we find that the two measures, the network similarity (S) and link stability (η), can be maximized for the same optimal coupling strength. This feature can be understood from the distribution of the correlation coefficients for the optimal coupling, which is bimodal with a distinct gap between the two distribution peaks, as shown in Fig. 1(e). While the gap is gradually narrowed as ε deviates from ε_o, the existence of the gap about ε_o is robust as any small variations in ε will not remove the gap. Since functional links are retrieved from the non-zero peak in the distribution, the functional network is stable for ε in the vicinity of ε_o. When ε is far from ε_o, the peaks are smeared and the distribution becomes unimodal, leading to ambiguities in the construction of the functional network. In this case, we say that the functional network is unstable.

Third, in retrieving the network structure using the CSA method, two problems may arise: unknown number of structural connections and unknown network size. For the former, we need to assume a number of links (e.g., based on some pre-knowledge about the network if available) and then calculate the stability measure by varying the coupling strength. For example, using the RN model studied in Sec. III and assuming there are $L' = N$ links in the network, we can analyze the consistency for these N connections using the CSA method. We find that, despite large variations in the connectivity stability, an optimal coupling strength always exists and its estimated value (1.6×10^{-2}) turns out to be slightly larger than that for the case of known network structure. For the case

of unknown network size, we choose a subset of nodes (e.g., $N' = 20$) and $L' = 20$ connections, which gives us a network of smaller size. Using the CSA method, we find that, within the interval $\varepsilon \in \left[9 \times 10^{-3}, 1.4 \times 10^{-2}\right]$, we have $S_{max} = 1$.

Fourth, the methodology developed in this paper for identifying and characterizing the consistency between functional and structural networks is for unweighted and undirected networks. It remains unknown whether weighted and directed complex networks can be treated. In studying heterogeneous networks such as SFNs and the cat brain network, we attribute the mismatched connection to the overlapping neighborhoods of the hub nodes, and suggest generalized synchronization as a possible source for the mismatch. However, the relationship between topological heterogeneity and network consistency remains to be investigated.

To summarize, using complex networks of coupled nonlinear oscillators, we have investigated the consistency between functional and structural connectivities in the physically and biologically relevant regime of weak coupling. Our main finding is that, regardless of the network structure and nodal dynamics, there exists an optimal coupling regime in which the consistency between the functional and structural networks is maximized. We develop a method (CSA) to identify the optimal coupling regime in practical situations of unknown network structure, and demonstrate that the method works well for both model and real-world networks. Our study provides new insights into the interplay between network structure and collective dynamical behaviors, which can be useful in understanding the working of physical and biological networks.

[1] E. Salinas and T. J. Sejnowski, Nat. Neurosci. **2**, 539 (2001); T. S. Gardner, D. di Bernardo, D. Lorenz, and J.J. Collins, Science **301**, 102 (2003); P. Fries, Trends Cogn. Sci. **9**, 474 (2005); A. Clauset, C. Moore, and M.E.J. Newman, Nature (London) **453**, 98 (2008); B. Barzel and A. Barabási, Nature Biotechnol. **31**, 720 (2013).

[2] K. J. Friston, Brain Connectivity **1**, 13 (2011).

[3] D. J. Watts and S. H. Strogatz, Nature (London) **393**, 440 (1998).

[4] T. Nishikawa, A. E. Motter, Y.-C. Lai, and F. C. Hoppensteadt, Phys. Rev. Lett. **91**, 014101 (2003); A. E. Motter, C. S. Zhou, and J. Kurths, Europhys. Lett. **69**, 334 (2005); M. Chavez, D.-U. Hwang, A. Amann, H. G. E. Hentschel, and S. Boccaletti, Phys. Rev. Lett. **94**, 218701 (2005); X.-G. Wang, Y.-C. Lai, and C.-H. Lai, Phys. Rev. E **75**, 056205 (2007).

[5] A. Arenas, A. Diaz-Guilera, J. Kurths, Y. Moreno, and C. S. Zhou, Phys. Rep. **469**, 93 (2008).

[6] M. Timme and J. Casadiego, J. Phys. A: Math. Theor. **47**, 343001 (2014).

[7] C. Fu, W. Lin, L. Huang, and X.-G. Wang, Phys. Rev. E **89**, 052908 (2014).

[8] A. Mritan and J. R. Banavar, Phys. Rev. Lett. **72** 1451 (1994).

[9] S. Guan, X.-G. Wang, X. Gong, K. Li, and C.-H. Lai, Chaos **19**, 013130 (2009).

[10] N. Friedman, Science **303**, 799 (2004).

[11] Z. Levnajić and A. Pikovsky, Phys. Rev. Lett **107**, 034101 (2011).

[12] L. Prignano and A. Díaz-Guilera, Phys. Rev. E **85**, 036112 (2012).

[13] P. Yang and Z. G. Zheng, Phys. Rev. E **90**, 052818 (2014).

[14] J. Ren, W. Wang, B. Li, and Y.-C. Lai, Phys. Rev. Lett. **104**, 058701 (2010).

[15] S. G. Shandilya and M. Timme, New J. Phys. **13**, 013004 (2011).

[16] W.-X. Wang, Y.-C. Lai, C. Grebogi, and J. Ye, Phys. Rev. X **1**, 021021 (2011); X. Han, Z.-S. Shen, W.-X. Wang, and Z.-R. Di, Phys. Rev. Lett. **114**, 028701 (2015).

[17] Z. Zhang, Z. Zheng. H. Niu, Y. Mi, S. Wu, and G. Hu, Phys Rev. E **91**, 012814 (2015).

[18] D. Yu, M. Righero, and L. Kocarev, Phys. Rev. Lett. **97**, 188701 (2006).

[19] A. Arenas, A. Díaz-Guilera, and C. J. Pérez-Vicente, Phys. Rev. Lett. **96**, 114102 (2006).

[20] M. Timme, EPL, **76**, 367 (2006).

[21] M. Timme, Phys. Rev. Lett. **98**, 224101 (2007).

[22] C. S. Zhou, L. Zemanová, C.C. Hilgetag, and J. Kurths, Phys. Rev. Lett. **97**, 238103 (2006).

[23] C. S. Zhou, L. Zemanová, G. Zamora-López, C. C. Hilgetag, and J. Kurths, New J. Phys. **9**, 178 (2007).

[24] V. Nicosia, M. Valencia, M. Chavez, A. Díaz-Guilera, and V. Latora, Phys. Rev. Lett. **110**, 174102 (2013).

[25] W.-X. Wang, Q.-F. Chen, L. Huang, Y.-C. Lai, and M. A. F. Harrison, Phys. Rev. E **80**, 016116 (2009).

[26] O. David and K. J. Friston, NeuroImage **20**, 1743 (2003).

[27] L. M. Pecora and T. L. Carroll, Phys. Rev. Lett. **80**, 2109 (1998); G. Hu, J. Z. Yang, and W. Liu, Phys. Rev. E **58**, 4440 (1998); L. Huang, Q.-F. Chen, Y.-C. Lai, and L. M. Pecora, Phys. Rev. E **80**, 036204 (2009).

[28] J. G. Restrepo, E. Ott, and B. R. Hunt, Phys. Rev. E **71**, 036151 (2005); X.-G. Wang, L. Huang, S. Guan, Y.-C. Lai, and C.-H. Lai, Chaos **18**, 037117 (2008).

[29] R. Albert and A. L. Barabási, Rev. Mod. Phys. **74**, 47 (2002).

[30] A. L. Barabási and R. Albert, Science **286**, 509 (1999).

[31] N. F. Rulkov, M. M. Sushchik, L. S. Tsimring, and H. D. I. Abarbane, Phys. Rev. E **51**, 980 (1995); Z. Zheng, X.-G. Wang, and M. C. Cross, Phys. Rev. E **65**, 056211 (2002).

[32] J. Gómez-Gardeñes, Y. Moreno, and A. Arenas, Phys. Rev. Lett. **98**, 034101 (2007); X.-G. Wang, S. Guan, Y.-C. Lai, B. Li, and C.-H. Lai, EPL, **88** 28001 (2009); C. Fu, Z. H. Zhang, M. Zhan, and X.-G. Wang, Phys. Rev. E **85**, 066208 (2012).

[33] X.-G. Wang, Eur. Phys. J. B **75**, 285 (2010).

[34] L. M. Pecora, F. Sorrentino, A. M. Hagerstrom, T. E. Murphy, and R. Roy, Nat. Commun. 5:4079 (2014).

[35] S. A. Bloomfield, D. Xin and T. Osborne, Vis. Neurosci. **14**, 565 (1997); B. W. Connors and M. A. Long, Annu. Rev. Neurosci. **27**, 393 (2004); C. E. Landisman and B. W. Connors, Science **310**, 1809 (2005).

[36] J. W. Scannell, G. A. P. C. Burns, C. C. Hilgetag, M. A. O'Neil1, and M. P. Young, Cereb. Cortex **9**, 277 (1999); O. Sporns and J. D. Zwi, Neuroinformatics **2**, 145 (2004).

[37] The Nepal electricity authority annual report 2011, avaliable at www.nea.org.np.

[38] O. E. Rössler, Phys. Lett. A **57**, 397 (1976).

[39] W. S. Kim, X.-M. Cui, C. N. Yoon, H. X. Ta, and S. K. Han, EPL, **96**, 20006 (2011).